Carbonate-Induced Electrosynthesis of Hydrogen Peroxide via Two-Electron Water Oxidation

Sotirios Mavrikis[a],[b]*, Maximilian Göltz[c], Prof. Stefan Rosiwal[c], Prof. Ling Wang[b] and Prof. Carlos Ponce de León[a]*

[a]Electrochemical Engineering Laboratory, Energy Technology Research Group, Faculty of Engineering and Physical Sciences, University of Southampton, Highfield Campus, University Road, Southampton, SO17 1BJ, United Kingdom

[b]National Centre for Advanced Tribology at Southampton (nCATS), Faculty of Engineering and Physical Sciences, University of Southampton, Highfield Campus, University Road, Southampton, SO17 1BJ, United Kingdom

[c]Materials Science and Engineering for Metals, Faculty of Engineering, Friedrich-Alexander University of Erlangen-Nürnberg, D-91058 Erlangen, Germany

*__Corresponding authors__: s.mavrikis@soton.ac.uk; capla@soton.ac.uk

Abstract

Electrochemical synthesis of hydrogen peroxide (H_2O_2), via the two-electron water oxidation reaction ($2e^-$ WOR), is an attractive method for the sustainable production of valuable chemicals in place of oxygen during water electrolysis. While the majority of $2e^-$ WOR studies have focussed on electrocatalyst design, little research has been carried out on the selection of the supporting electrolyte. In this work, we investigate the impact of potassium carbonate (K_2CO_3) electrolytes, and their key properties, on H_2O_2 production. We find that at electrolyte pH values (> 9.5) where the carbonate anion (CO_3^{2-}) is prevalent in the mixture, a 26.5% increase in the Faraday efficiency (%*FE*) for H_2O_2 production is achieved, compared to bicarbonate (HCO_3^-) dominant solutions. Utilising boron-doped diamond (BDD) in highly concentrated K_2CO_3 solutions, current densities of up to 511 mA cm^{-2} (in 4 M) and %*FE*s of 91.5% (in 5 M) can be attained. The results presented in this work highlight the influence of CO_3^{2-} on electrochemical H_2O_2 generation via the $2e^-$ WOR and provide novel pathways to produce desirable commodities at the anode during electrochemical water splitting.

Keywords: boron-doped diamond (BDD); carbonate (CO_3^{2-}); electrochemistry; electrolyte; hydrogen peroxide (H_2O_2); oxidation; two-electron water oxidation reaction ($2e^-$ WOR); water chemistry

Introduction

Electrochemical water splitting, powered by renewable energy, is an attractive method for the emission-free production of sustainably sourced hydrogen (H_2) at the cathode, and oxygen (O_2) at the anode.[1,2] While the electrosynthesis of H_2 has received widespread attention due to its promise as a green energy carrier,[3] the production and low market value of O_2 is considered a major technological and economic bottleneck for the implementation of water electrolysis on a larger scale.[4] The attention of researchers has thus shifted toward producing high-value and coveted chemicals at the anode in place of O_2. One such alternative is hydrogen peroxide (H_2O_2), a powerful green oxidising agent with applications in paper and textile bleaching, water treatment, chemical synthesis, and electrical energy generation.[5,6] Anodic H_2O_2 production can be achieved via the two-electron water oxidation reaction (2e^- WOR) (Equation 1), an unorthodox method for H_2O_2 electrosynthesis given the thermodynamic favourability of the O_2 evolution and H_2O_2 oxidation reactions (Equations 2, 3).

$$2H_2O \rightleftharpoons H_2O_2 + 2H^+ + 2e^- \qquad E^0 = 1.76\ \text{V } \textit{vs.}\ \text{RHE} \qquad (1)$$

$$2H_2O \rightleftharpoons O_2 + 4H^+ + 4e^- \qquad E^0 = 1.23\ \text{V } \textit{vs.}\ \text{RHE} \qquad (2)$$

$$H_2O_2 \rightleftharpoons O_2 + 2H^+ + 2e^- \qquad E^0 = 0.67\ \text{V } \textit{vs.}\ \text{RHE} \qquad (3)$$

Consequently, the majority of 2e^- WOR studies have focussed on the development of suitable catalytic materials that will drive the selectivity of water oxidation toward H_2O_2.[7] Equally important to the electrocatalyst, however, is the aqueous supporting electrolyte used, which will impact the production, and stability, of H_2O_2.[8] Highly concentrated hydrogen carbonate, or bicarbonate (HCO_3^-), solutions have been identified as suitable electrolytes for H_2O_2 production,[9] with 2 M $KHCO_3$ being well established in the 2e^- WOR literature as the convention for aqueous supporting electrolytes.[10–17] Recently, a transition toward carbonate (CO_3^{2-}) based solutions, for H_2O_2 production, has been noticed, and prominent studies have reported increased H_2O_2 production rates in Na_2CO_3,[18] or K_2CO_3/$KHCO_3$ mixtures.[19] A dedicated study on the influence of carbonate electrolytes and their key properties (concentration, pH, conductivity) on H_2O_2 electrosynthesis via the 2e^- WOR has yet to be carried out.

Accordingly, in this work, an investigation is made on the promotive effect of CO_3^{2-} to electrochemically generate H_2O_2 via the 2e^- WOR in potassium carbonate, K_2CO_3, electrolytes using boron-doped diamond-coated niobium anodes (herein designated 'BDD/Nb'). Initially, the electroactive surface area (EASA) of the BDD films used, a key electrocatalyst characteristic often overlooked in the 2e^- WOR literature, is determined for the rational reporting of important 2e^- WOR performance parameters like the current density (mA cm^{-2}) or the production rate of H_2O_2 (µmol cm^{-2} min^{-1}). It is found that the EASA is notably larger than the commonly used geometric surface area of the catalyst and as such, all parameters related to the surface area are normalised to the EASA. Next, to evaluate the impact of H_2CO_3, HCO_3^- and CO_3^{2-} on H_2O_2 production, electrochemical measurements are carried out in mixed K_2CO_3/$KHCO_3$ where it is found that a shift from pH 9, where HCO_3^- is the dominant dissolved inorganic carbon species, to pH 10, where CO_3^{2-} is prevalent, will result in a 26.5% increase in the faradaic efficiency (%*FE*) for H_2O_2 production. High Tafel slope coefficients (303 – 510 mV dec^{-1}) calculated for BDD in the mixed electrolyte at pH ~ 9.85 can likely be attributed to the formation of hydroxyl radicals ($HO^\bullet$) at the surface of BDD. Further experiments in highly concentrated K_2CO_3 solutions using BDD revealed that current densities of up to 511 mA cm^{-2} (4 M K_2CO_3) and %*FE*s of 91.5% (5 M K_2CO_3) can be attained alongside an experimentally observed decrease in oxygen

evolution (anodic bubble formation) during electrolysis. Finally, a rudimentary examination of four popular H_2O_2 detection methods revealed that titration with potassium permanganate ($KMnO_4$) is insusceptible to interferences from other oxidants ($Na_2S_2O_8$) or anions (CO_3^{2-}) present in the aliquot, thus deeming it a reliable method for the quantification of electrochemically-generated H_2O_2 via the $2e^-$ WOR in K_2CO_3 solutions. These findings highlight the positive impact of CO_3^{2-} on efficient anodic H_2O_2 electrosynthesis, an appealing alternative to O_2 evolution for the advancement of water electrolysis technologies.

Results and Discussion

Prior to investigating the $2e^-$ WOR performance in carbonate solutions, the effective electroactive surface area (EASA) of the BDD catalytic films should be quantified given its influence on the electrochemical activity of the BDD/Nb electrodes. Cyclic voltammetry (CV) of a 1 mM ferricyanide and 1 mM ferrocyanide, $[Fe(CN)_6]^{3-/4-}$ redox system, a standard method to determine the EASA of BDD films, is carried out for all six anodes at scan rates between 10 and 120 mV s^{-1}. The EASA is estimated by analysing the resulting curves (Figure 1 a–f) using the Randles–Ševčík equation (Equation S4).[20] It is found that the EASA of the six BDD films is on average 1.6 times larger than their respective geometric surface areas (Figure S1) due to the rough nature of the films. The estimated EASAs of the BDD/Nb anodes can be found in Table S2 of the Supporting Information, and these surface area values will be used when reporting the current density (mA cm^{-2}) and H_2O_2 production rate (µmol cm^{-2} min^{-1}) in this work. It should be noted that the CV-peak method used here measures the EASA at a particular potential corresponding to the formation of the Nernst diffusion layer and not the period of time between the appearance and full formation of the diffusion layer.[21] Thus this method will account for the primary large pores of the surface of the catalyst, but may exclude the surface area of secondary pores smaller than the thickness of the Nernst diffusion layer. Given that the estimated EASA is larger than the measured geometric surface area, accurate reporting of the $2e^-$ WOR performance of proposed electrocatalysts, as well as valid comparisons of $2e^-$ WOR studies, both require current densities and production rates to be normalised to the geometric and real surface areas of the investigated catalytic films.[22] Amongst the six tested anodes, the lowest peak-to-peak separation value, ΔE_p, was found for BDD/Nb-6 and was equal to 71 mV, at a scan rate of 10 mV s^{-1}, only slightly higher than the ideal value of approximately 57 mV expected for a reversible one-electron couple, and well within the range for typical experimental values (70 – 80 mV). Similar values are recorded for all BDD/Nb electrodes (Table S3) with the exception of BDD/Nb-1 which was found to have a less-reversible ΔE_p of 129 mV, a value attributed, most likely, to its lower doping level compared to the other BDD films.[23] Anodes BDD/Nb-2 to BDD/Nb-6 are doped sufficiently (B: $1.09 – 2.86 \times 10^{21}$ atoms cm^{-3}) to behave as metal-like electrodes.[20,24] Given that the peak potential changes slightly with an increase in the scan rate, particularly evident in Figure 1 (a), it can be concluded that the BDD/Nb electrodes possess a quasi-reversible character, agreeing with the existing literature.[25]

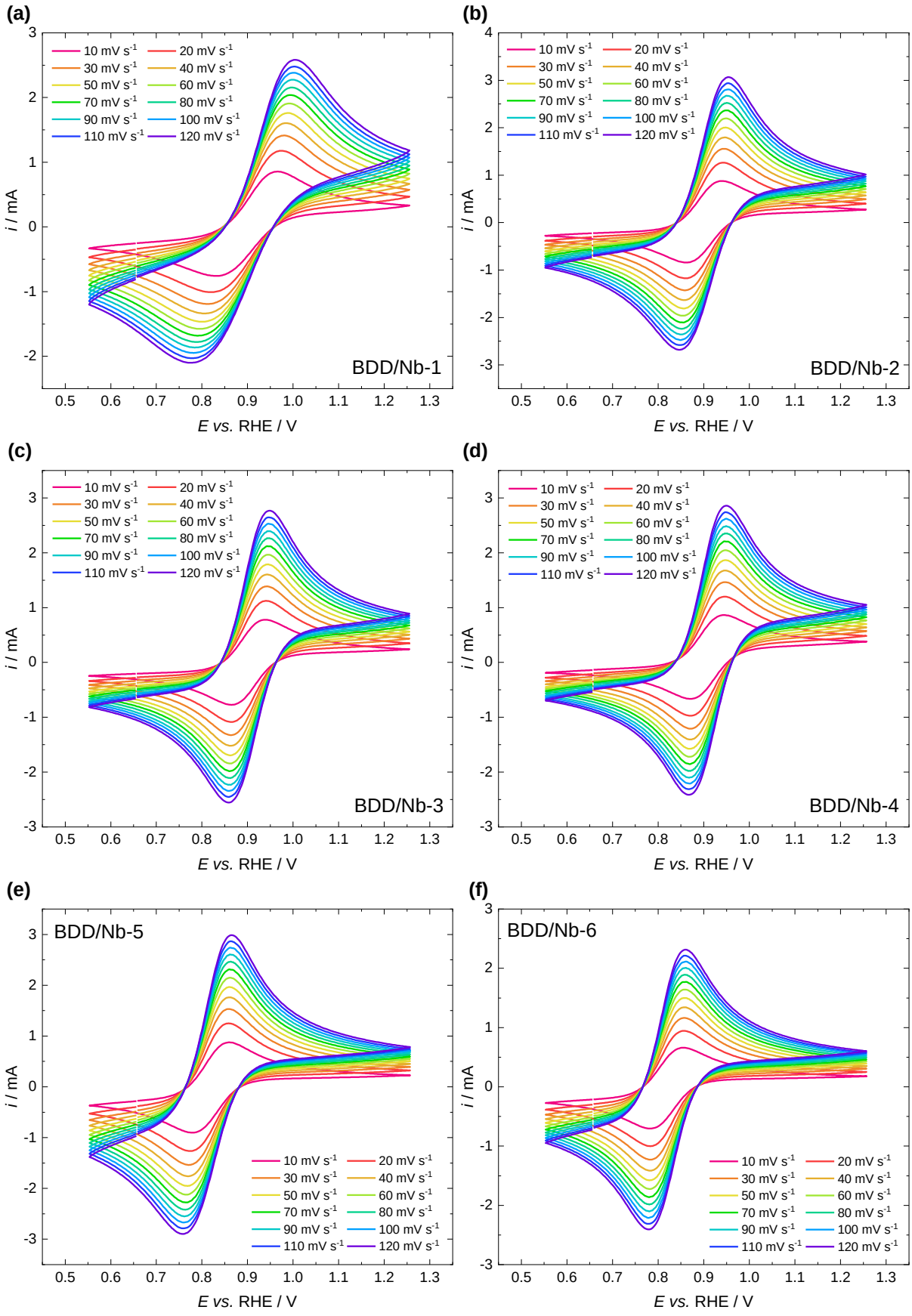

Figure 1 Cyclic voltammograms (CVs) of a 1 mM potassium ferricyanide and 1 mM potassium ferrocyanide, $K_3[Fe(CN)_6]/K_4[Fe(CN)_6]$ redox system in 1 M potassium chloride, KCl, for six BDD/Nb anodes. All measurements were carried out at scan rates of 10 – 120 mV s^{-1}. **(a)** BDD/Nb-1. **(b)** BDD/Nb-2. **(c)** BDD/Nb-3. **(d)** BDD/Nb-4. **(e)** BDD/Nb-5. **(f)** BDD/Nb-6.

The $2e^-$ WOR performance of BDD/Nb-4 to electro-synthesise H_2O_2 is investigated in mixed bicarbonate/carbonate solutions that possess pH values ranging between 7 – 12 at an applied constant j of 100 mA cm^{-2} for a duration of 5 min. The pH range is selected to determine which dissolved inorganic carbon species (H_2CO_3, HCO_3^-, CO_3^{2-}), based on the Bjerrum plot for carbonate systems,[26] has the largest influence on H_2O_2 generation. The selectivity and activity of BDD/Nb-4 for the $2e^-$ WOR at each pH value of the electrolyte are assessed via the H_2O_2 concentration, %*FE* and H_2O_2 production rate (Figure 2a – inset) as depicted in Figure 2 (a).

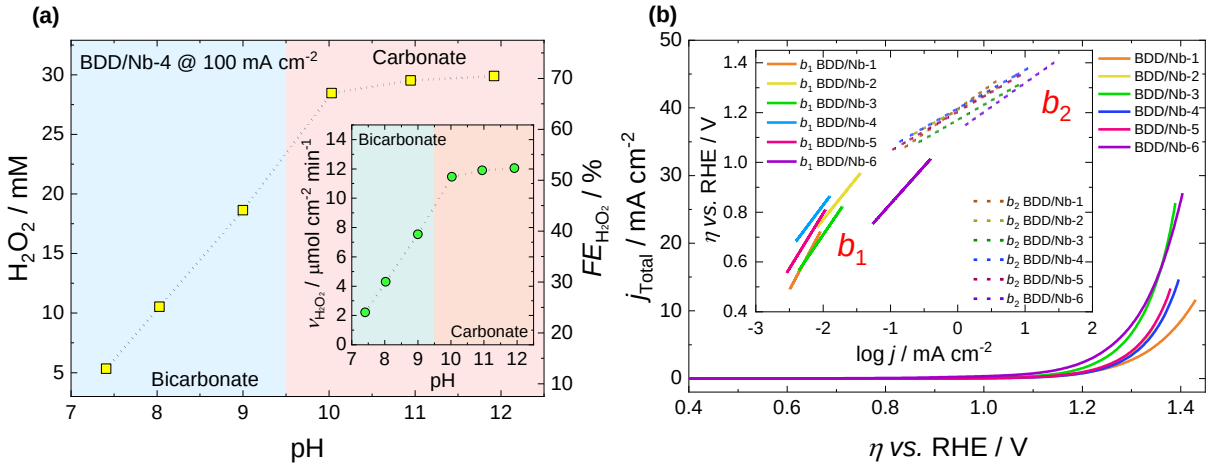

Figure 2 (a) H_2O_2 concentration achieved (left y axis), and %*FE* for H_2O_2 synthesis (right y axis), as a function of the pH of a bicarbonate/carbonate electrolyte using BDD/Nb-4 at an applied current of 100 mA cm^{-2} for 5 min. The inset graph shows the H_2O_2 production rate (μmol cm^{-2} min^{-1}) of BDD/Nb-4 in bicarbonate/carbonate versus the electrolyte pH at j = 100 mA cm^{-2}. **(b)** Current density – overpotential curves (for the oxygen evolution reaction), following ohmic drop corrections, recorded in 1 M K_2CO_3/1 M $KHCO_3$, using six BDD/Nb electrodes, at a scan rate of 5 mV s^{-1}. The inset graph depicts the Tafel plots of the six BDD/Nb anodes.

An increase in all three $2e^-$ WOR performance parameters is observed as the pH of the solution increases from 7 to 12, coinciding with an increase in the molar fraction of CO_3^{2-}. A notable increase in H_2O_2 production occurs in the pH region above 9.5 (red coloured area of Figure 2a), where CO_3^{2-} is the dominant dissolved inorganic carbon species in the electrolyte, with the %*FE* for H_2O_2 production increasing from 44% at pH 9 to 70.5% at pH 12. Peak values for the H_2O_2 concentration (29.9 mM) and production rate (12.04 μmol cm^{-2} min^{-1}) are also attained at pH 12, highlighting the influential role of CO_3^{2-} on the $2e^-$ WOR. Linear sweep voltammograms (LSVs) of the six BDD/Nb electrodes (Figure 2b), as a function of the overpotential for the four-electron oxygen evolution reaction, are recorded in 1 M K_2CO_3/1 M $KHCO_3$, at a pH of around 9.85, where the influence of CO_3^{2-} is more pronounced on H_2O_2 production. The anodic polarisation curves are corrected for ohmic potential drop, jR, based on the established method proposed by Shub and Reznik (Equation S8),[27] where the total area-specific uncompensated resistance of the system is determined by plotting $\Delta\eta$ Δj^{-1} versus j^{-1} and deriving the intercept of the slope at current densities where the jR drop prominently contributes to the overpotential (Figure S2). Similar to observations made by the Comninellis research group,[28,29] two distinct Tafel slopes are discerned in the overpotential region above 0.4 V *vs.* RHE (Figure 2b – inset). In the high overpotential region above 1 V *vs.* RHE, Tafel slope coefficients (b_2) between 150 – 195 mV dec^{-1} are obtained for the six BDD/Nb anodes (Table S4), slightly higher than the theoretical value of 120 mV dec^{-1} for water discharge at 25 °C.[30] In the lower overpotential region (below 1 V *vs.* RHE), Tafel slope coefficients (b_1) of 303 – 510 mV dec^{-1} are obtained for the investigated BDD films. High Tafel coefficients (200 – 500 mV dec^{-1}) recorded for BDD in acidic electrolytes in previous studies have been attributed to the semi-metal or semiconductor character of the investigated BDD films,[31–33]

however, heavily-doped BDD (10^{21} atoms cm^{-3}), such as the electrodes used in this work, resembles a metal. Thus, the high Tafel slope coefficients for oxygen evolution can likely be attributed to the weak interaction of the hydroxyl radical ($HO^{\bullet}$), the intermediate formed following the one-electron oxidation of water (Equation 4), with the surface of BDD.[30] This postulation is further supported in studies carried out by García-Osorio et al., where it is reported that Tafel slope coefficients larger than 100 mV dec^{-1} are associated with $HO^{\bullet}$ formation, which is particularly prominent using BDD.[34,35]

$$H_2O \rightleftharpoons HO^{\bullet} + H^+ + e^- \qquad E° = 2.73 \text{ V } \textit{vs.} \text{ RHE} \qquad (4)$$

The influence of carbonate on H_2O_2 generation is further scrutinised by performing chronopotentiometry in seven aqueous K_2CO_3 solutions with concentrations between 0.1 – 5 M using BDD/Nb-4. Similar experiments in $KHCO_3$ solutions can additionally be seen in Figure S3.

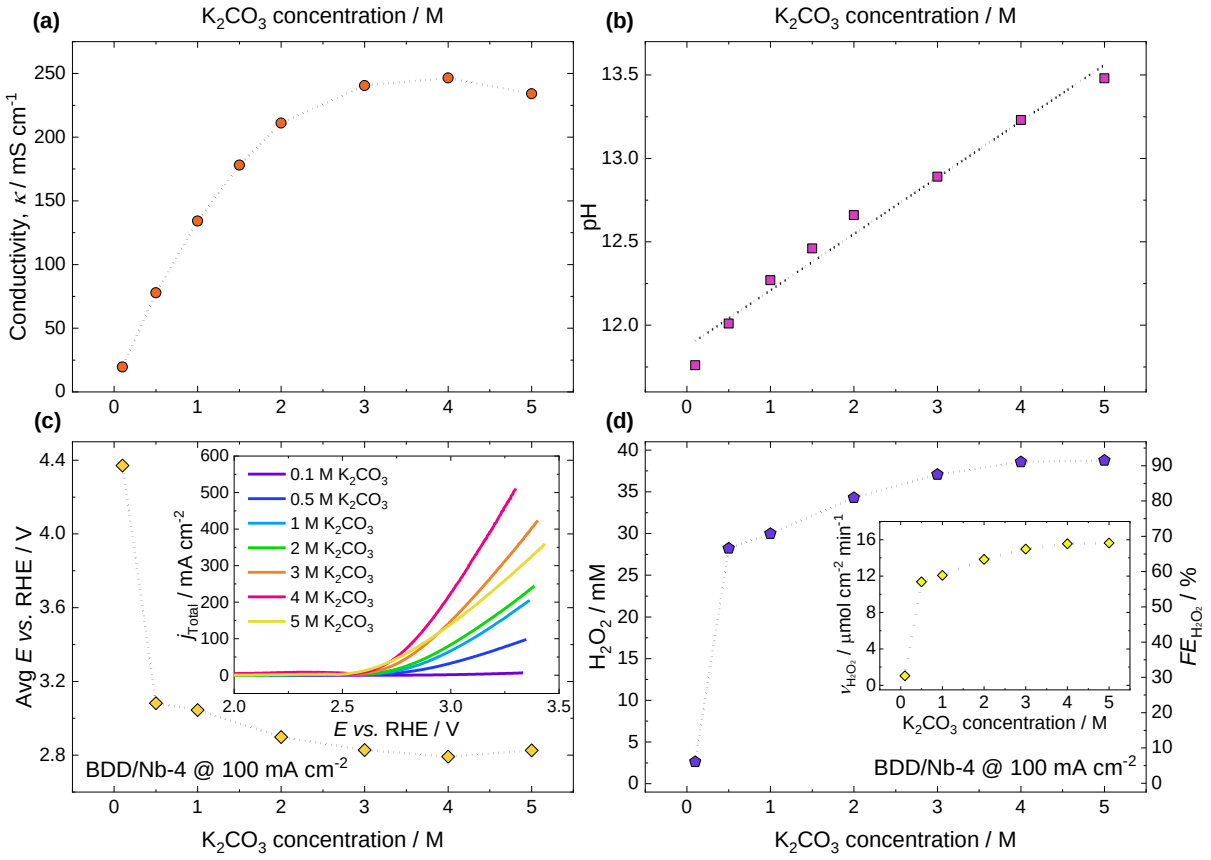

Figure 3 (a) Specific conductance (mS cm^{-1}) of K_2CO_3 solutions as a function of the concentration of K_2CO_3 (M). **(b)** pH of K_2CO_3 *vs.* the concentration of the electrolyte. **(c)** Average recorded working electrode potential of BDD/Nb-4 as a function of the concentration of K_2CO_3, upon applying a constant *j* of 100 mA cm^{-2} for 5 min. The inset graph shows the current density – potential curves recorded at a scan rate of 20 mV s^{-1} in seven different concentrations of K_2CO_3 using BDD/Nb-4. **(d)** Accumulated H_2O_2 (left y axis) and %*FE* for H_2O_2 production (right y axis) as a function of K_2CO_3 following chronoamperometry at 100 mA cm^{-2} for 5 min using BDD/Nb-4. The inset graph depicts the production rate of H_2O_2 using BDD/Nb-4 *vs.* the concentration of K_2CO_3.

Figure 3 (a) shows the electrical conductivity of the different K_2CO_3 mixtures, a key parameter for evaluating the electrochemical performance of a $2e^-$ WOR system, versus the molar concentration of the electrolyte. The conductivity of the solution initially increases with an increase in the electrolyte

concentration, analogous to the number of ions per unit volume of the electrolyte, reaching a maximum value of 246.5 mS cm^{-1} at a molar concentration of 4 M K_2CO_3, before gradually decreasing. This slight conductivity decrease can likely be attributed to a decrease in the distance between the cations and anions present in the mixture, in addition to the formation of non-conductive ion pairs, resulting in an overall decrease in the number of free ions participating in conduction.[36] Concerning the pH of the electrolyte (Figure 3b), a linear increase is observed as the concentration of K_2CO_3 increases, leading to the formation of strong alkaline solutions (pH > 13) particularly at concentrations of around 4 – 5 M K_2CO_3. The LSVs of BDD/Nb-4 shown in Figure 3 (c) – inset indicate that attained current densities are proportional to the conductivity of the respective K_2CO_3 solution, with BDD/Nb-4 achieving a peak *j* of approximately 511 mA cm^{-2} at just 3.3 V *vs.* RHE in 4 M K_2CO_3, the most conductive of the carbonate electrolytes investigated in this work. Consequently, upon carrying out 5 min constant current (100 mA cm^{-2}) electrochemical measurements using BDD/Nb-4 in the seven K_2CO_3 solutions, it is found that the average recorded working electrode potential decreases rapidly between 0.1 M K_2CO_3 (4.37 V *vs.* RHE) and 0.5 M K_2CO_3 (3.08 V *vs.* RHE) and moderately between 0.5 – 5 M K_2CO_3, in a manner that is proportional to the conductivity of the solution (Figure 3 c) The lowest potential of 2.79 V *vs.* RHE is recorded in 4 M K_2CO_3 at 100 mA cm^{-2} corresponding to an overpotential of just 1030 mV for the 2e^- WOR. Regarding the activity and selectivity of BDD/Nb-4 in different K_2CO_3 solutions at 100 mA cm^{-2}, the opposite trend is observed regarding H_2O_2 accumulation (Figure 3d), where a swift increase in H_2O_2 occurs upon increasing the concentration of K_2CO_3 from 0.1 M to 0.5 M, after which a more gradual increase is observed until 5 M K_2CO_3, where H_2O_2 accumulation and production are both optimal, corresponding to values of 39 mM and 15.6 µmol cm^{-2} min^{-1}, respectively (Figure 3 d – inset). A peak %*FE* of 91.5% for H_2O_2 production is additionally attained in 5 M K_2CO_3, amongst the highest values reported to date for the 2e^- WOR (Figure S4). The observations made in this work regarding the influence of high concentrations of K_2CO_3 on anodic H_2O_2 production agree with the experimental findings and theoretical predictions made in previous studies,[19,37–40] where it has been proposed that $HO^\bullet$ radicals, generated via the 1e^- WOR at the surface of BDD, react with CO_3^{2-}/HCO_3^- in the aqueous electrolyte to form the transient species $CO_3^{\bullet-}$ (Equation 5). Oxidation of the carbonate radical will lead to the production of peroxymonocarbonate, HCO_4^- (Equation 6), the subsequent hydrolysis of which will result in the formation of H_2O_2 and HCO_3^- (Equation 7). Further validation of this hydrolysis step, whereby oxygen atoms are exchanged between water and carbonate ions, would require oxygen ^{18}O isotope analysis, based on a recent report.[18] Under alkaline conditions, bicarbonate (or dissolved CO_2 in the electrolyte) will be converted to carbonate (Equation 8) thus completing the reaction cycle. A simplified suggested pathway for H_2O_2 generation in carbonate solutions at the anode can be seen in Scheme 1.

$$CO_3^{2-} + HO^\bullet \rightarrow CO_3^{\bullet-} + OH^- \quad (5)$$

$$CO_3^{\bullet-} + HO^\bullet \rightarrow HCO_4^- \quad (6)$$

$$HCO_4^- + H_2O \rightarrow H_2O_2 + HCO_3^- \quad (7)$$

$$HCO_3^- \rightarrow CO_3^{2-} + H^+ \quad (8)$$

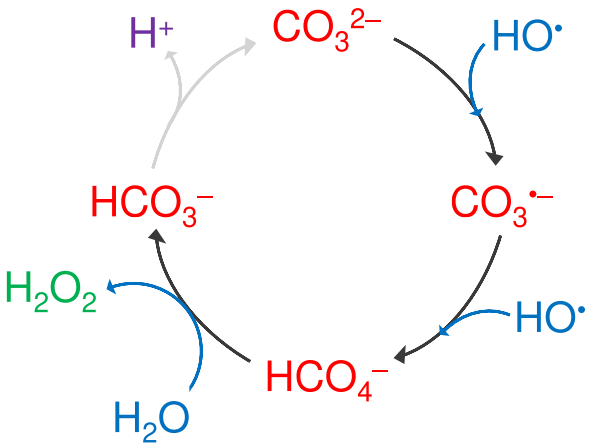

Scheme 1 Simplified hypothetical reaction mechanism for H_2O_2 production using BDD in aqueous carbonate solutions.

Finally, a simple comparison of prominent procedures for H_2O_2 quantification in the WOR literature is made to assess the accuracy of the various detection methods employed and the resulting H_2O_2 concentrations and *%FEs* reported. Four typical H_2O_2 determination methods are investigated: titration with ceric sulfate ($Ce(SO_4)_2$), titration with potassium permanganate ($KMnO_4$), semi-quantitative H_2O_2 determination test strips (Quantofix 1 – 100 mg L^{-1} H_2O_2) and UV-vis spectrophotometry using titanium oxysulfate ($TiOSO_4$) (Figure S5). Detailed descriptions of each quantification method are provided in the SI. Five solutions containing known concentrations of H_2O_2 and another oxidising agent, sodium persulfate ($Na_2S_2O_8$), for possible interference-effect observations, are prepared for the determination of the H_2O_2 concentration.[41] The prepared H_2O_2 concentration range is 20 – 100 mM (increments of 20 mM per solution), while the $Na_2S_2O_8$ concentration range is 30 – 150 mM (increments of 30 mM per solution). Thus, for example, the first investigated solution will have an H_2O_2 concentration of 20 mM and an $Na_2S_2O_8$ concentration of 30 mM, corresponding to a total oxidants' concentration of 50 mM. The total oxidants concentration range is 50 – 250 mM (increments of 50 mM per solution). A comparison of the different H_2O_2 detection methods for known concentrations of H_2O_2 can be seen in Figure 4 (a). The two titration methods both demonstrate high precision toward H_2O_2, exclusively, with a relative error of up to 3.5% for $Ce(SO_4)_2$ titration and up to 6% for $KMnO_4$ titration. Additionally, H_2O_2 concentration deviations for $Ce(SO_4)_2$ titration are much lower (± 0.1 – 1 mM) compared to $KMnO_4$ titration (± 0.2 – 5 mM). The $TiOSO_4$ spectrophotometric method is found to be less precise for H_2O_2 quantification, compared to the titration methods, possibly due to interferences from $Na_2S_2O_8$ with relative errors of up to 34% at lower H_2O_2 concentrations. In each prepared solution tested, $TiOSO_4$ spectrophotometry exaggerated the H_2O_2 concentration, with deviations ranging between 2 – 8 mM. The semi-quantitative H_2O_2 detection strips were found to be extremely sensitive to $Na_2S_2O_8$ present in the H_2O_2 mixture, reporting the total oxidants present in the solution as H_2O_2. Relative errors of up to 150% were common for all the tested solutions using the colorimetric strips, given their susceptibility to false positives from strong oxidants present in the mixture as stated by the manufacturer.

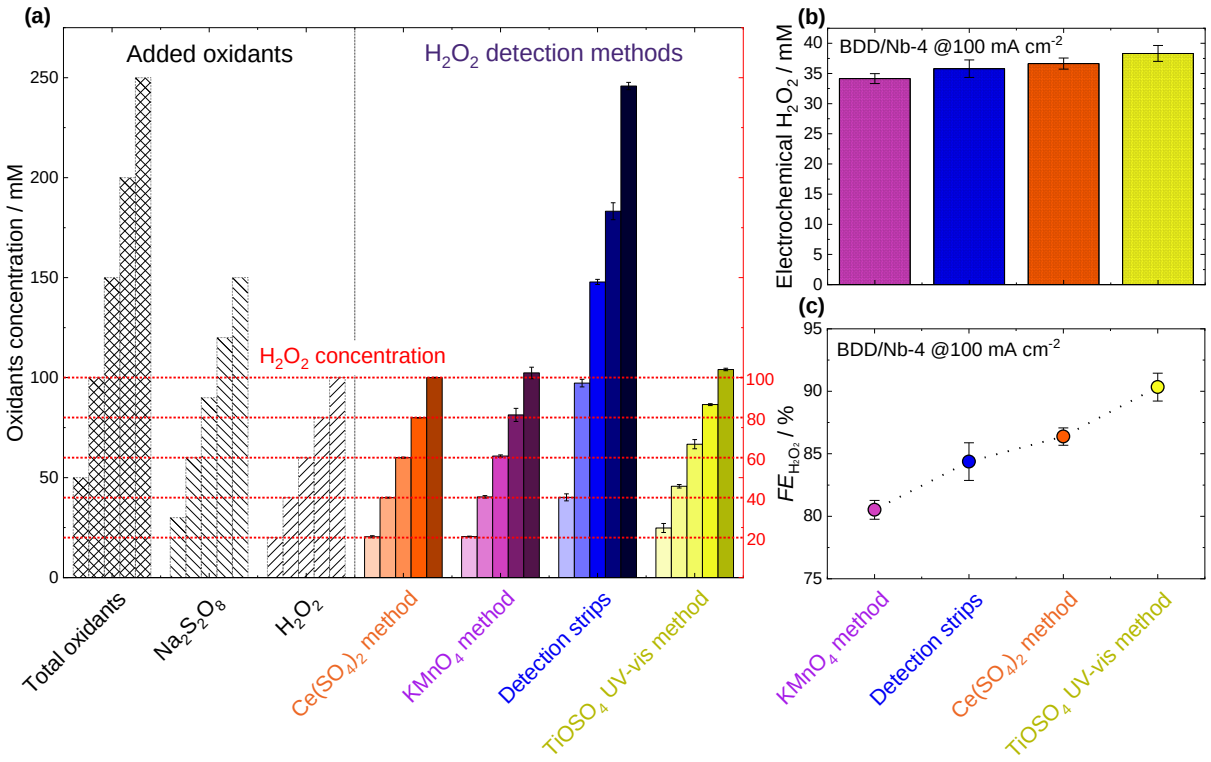

Figure 4 (a) Determination of the H_2O_2 concentration in five prepared dual oxidant ($Na_2S_2O_8$ + H_2O_2) solutions using four prominent H_2O_2 detection methods: $Ce(SO_4)_2$ titration, $KMnO_4$ titration, semi-quantitative H_2O_2 detection strips and $TiOSO_4$ spectrophotometry. **(b)** Difference in the H_2O_2 concentration measured using the four detection methods following chronopotentiometry in 2 M K_2CO_3 using BDD/Nb-4. **(c)** Difference in the %*FE* for H_2O_2 production calculated using the four detection methods following chronopotentiometry in 2 M K_2CO_3 using BDD/Nb-4.

Next, chronopotentiometry, using BDD/Nb-4 in 2 M K_2CO_3 at an applied current of 100 mA cm^{-2} for 5 min, was carried out to evaluate the accuracy of the detection methods for electrochemically generated H_2O_2 in carbonate (Figure 4b). Titration with $KMnO_4$ resulted in an H_2O_2 concentration of approximately 34 mM, while the colorimetric strips and $Ce(SO_4)_2$ titration both gave slightly higher H_2O_2 concentration values of 35.8 mM and 36.6 mM, respectively. The $TiOSO_4$ spectrophotometric method resulted in an H_2O_2 concentration of 38.3 mM, a 4 mM deviation from $KMnO_4$ titration. The variance in the quantified H_2O_2 concentrations is further accentuated when calculating the %*FE* for H_2O_2 production following the electrochemical measurement (Figure 4c), where the %*FE* difference between $KMnO_4$ titration (80.5%) and $TiOSO_4$ (90.3%) spectrophotometry is almost 10%, a substantial disparity between the two detection methods. It has been previously reported that the $TiOSO_4$ method may be susceptible to interferences from anions like CO_3^{2-} present in the electrolyte.[42,43]

Conclusion

In conclusion, this work has emphasised the positive impact of K_2CO_3 electrolytes on the 2e^- WOR to electrochemically generate H_2O_2 using BDD/Nb anodes. By initially determining the electroactive surface area of the catalyst used, a more rational manner for reporting important 2e^- WOR performance indicators, like the current density or H_2O_2 production rate, is presented. Electrochemical measurements across a wide pH range found that, upon shifting the pH of the bicarbonate/carbonate electrolyte toward values (pH > 9.5) where the CO_3^{2-} anion becomes the dominant dissolved inorganic carbon species, a 26.5% increase in the %*FE* for H_2O_2 electrosynthesis is attained. High Tafel slope coefficient values, between 303 – 510 mV dec^{-1}, determined in the low OER overpotential region, were found to be consistent with the literature for $HO^{\bullet}$ generation. Further experiments in highly concentrated K_2CO_3 solutions revealed that an increase in the concentration and conductivity of the electrolyte will augment H_2O_2 production, with current densities reaching up to 511 mA cm^{-2} at just 3.3 V *vs.* RHE in 4 M K_2CO_3, and %*FE*s peaking at 91.5% in 5 M K_2CO_3. Additionally, a brief evaluation of four prominent H_2O_2 concentration determination methods revealed that standard titration with $KMnO_4$ was least susceptible to interferences in H_2O_2-carbonate aliquots and should be regarded as a reliable method for H_2O_2 quantification in K_2CO_3 for the 2e^- WOR. The impressive redox catalytic role of CO_3^{2-}, demonstrated in this study, on H_2O_2 production in K_2CO_3 solutions has highlighted the significance of the supporting electrolyte for the 2e^- WOR. An appropriate electrocatalyst-electrolyte combination may help drive the selectivity of the water oxidation reaction toward H_2O_2 instead of O_2 thus allowing for the sustainable electrochemical production of two valuable commodities (H_2 and H_2O_2) during water electrolysis. This present work at the anode may also be integrated with the two-electron oxygen reduction reaction (2e^- ORR) at the cathode,[44–48] to achieve high rate electrosynthesis of H_2O_2 at both electrodes using a single pass of charge. Given that anodic electrochemical generation of H_2O_2 in carbonate is still in its infancy, further research into the precise role of CO_3^{2-} on the reaction mechanism is necessary.

Experimental Section

All electrochemical measurements were carried out in a custom-built, two-compartment, three-electrode and low-volume glass cell (Scheme 2) using a Metrohm Autolab PGSTAT302N potentiostat connected to an Autolab Booster 20A. The two compartments were separated by a Nafion 115 cation exchange membrane pre-treated in sulfuric acid (H_2SO_4) and deionised water and stored in deionised water. The working electrode (WE) compartment contained the BDD/Nb anode (Table S1), a mercury/mercury oxide (Hg|HgO, 1 M NaOH) reference electrode and a borosilicate-coated magnetic stirring bar to stir the anolyte at approximately 600 rpm. The counter electrode (CE) compartment contained a 25 cm^2 platinum mesh cathode. Each compartment had an electrolyte volume of 25 mL. For chronopotentiometry measurements, an electrical current of 100 mA cm^{-2} was applied constantly for 5 min. All electrochemically generated H_2O_2 was quantified via the standard $KMnO_4$ titration method for every measurement except for the *H_2O_2 Detection Methods* experiment shown in Figure 4, where three other determination methods ($Ce(SO_4)_2$ titration, $TiOSO_4$ UV-vis spectrophotometry and semi-quantitative H_2O_2 test strips) were additionally implemented. A complete description of the H_2O_2 detection methods used can be found above Figure S5 in the SI. The conversion of the working electrode potential to RHE, the calculation of the *%FE* for H_2O_2 production, and the *jR* drop compensation calculations can be found in the SI via Equation S1, Equation S2 and Equation S8, respectively.

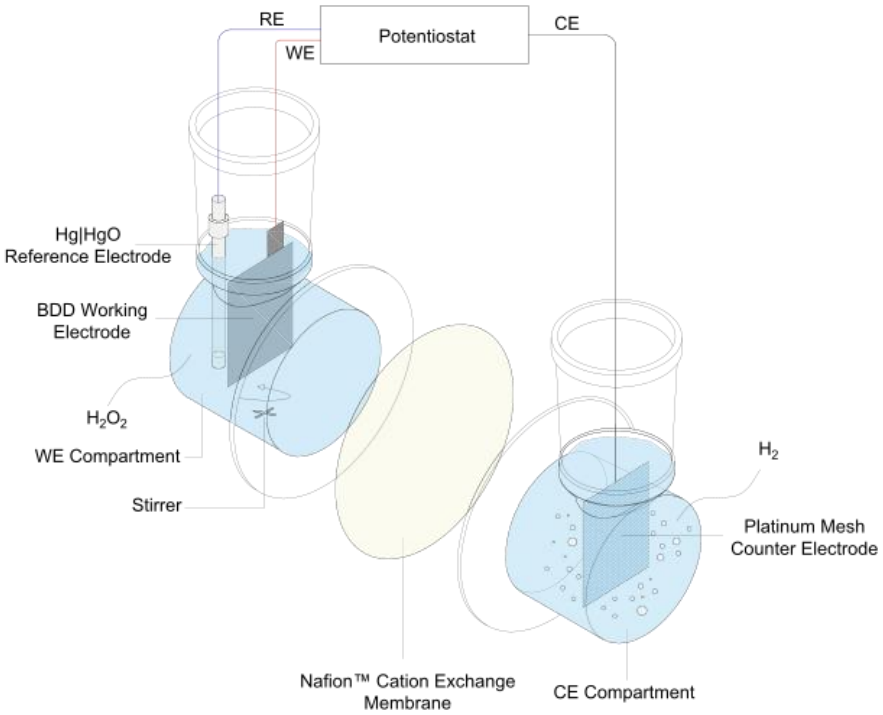

Scheme 2 Illustration of the custom-made, two compartment and low volume cell used for electrochemical measurements.

Author Contributions

S.M: conceptualisation, investigation, methodology, visualisation, writing – original draft and review & editing. M.G: electrode fabrication, writing – review & editing. S.R: electrode fabrication, writing – review & editing. L.W: supervision, writing – review & editing. C.P.d.L: conceptualisation, supervision, writing – review & editing.

Acknowledgements

The University of Southampton is part of the CO_2-based electrosynthesis of ethylene oxide (CO_2EXIDE) project consortium, which receives funding from the European Union's Horizon 2020 research and innovation program in cooperation with the sustainable process industry through a resource and energy efficiency (SPIRE) initiative under grant agreement no. 768789. The authors acknowledge Moritz Wegener from Schaeffler Technologies AG for the financial support, Dmitry Bavykin and Julian Wharton from the University of Southampton for their suggestions regarding the methodology, and Andreas Zervas from the University of Patras for assisting with the visualisation of the experimental setup.

Conflicts of Interest

The authors declare no conflicts of interest.

References

[1] S. Anantharaj, S. Noda, *Small* **2020**, *16*, 1905779.

[2] A. Govind Rajan, J. M. P. Martirez, E. A. Carter, *ACS Catal.* **2020**, *10*, 11177–11234.

[3] P. J. McHugh, A. D. Stergiou, M. D. Symes, *Adv. Energy Mater.* **2020**, *10*, 2002453.

[4] K. Wenderich, W. Kwak, A. Grimm, G. J. Kramer, G. Mul, B. Mei, *Sustain. Energy Fuels* **2020**, *4*, 3143–3156.

[5] J. M. Campos-Martin, G. Blanco-Brieva, J. L. G. Fierro, *Angew. Chemie - Int. Ed.* **2006**, *45*, 6962–6984.

[6] L. An, T. Zhao, X. Yan, X. Zhou, P. Tan, *Sci. Bull.* **2015**, *60*, 55–64.

[7] S. Mavrikis, S. C. Perry, P. K. Leung, L. Wang, C. Ponce de León, *ACS Sustain. Chem. Eng.* **2021**, *9*, 76–91.

[8] J. Liu, Y. Zou, B. Jin, K. Zhang, J. H. Park, *ACS Energy Lett.* **2019**, *4*, 3018–3027.

[9] K. Fuku, Y. Miyase, Y. Miseki, T. Gunji, K. Sayama, *ChemistrySelect* **2016**, *1*, 5721–5726.

[10] K. Fuku, K. Sayama, *Chem. Commun.* **2016**, *52*, 5406–5409.

[11] S. Y. Park, H. Abroshan, X. Shi, H. S. Jung, S. Siahrostami, X. Zheng, *ACS Energy Lett.* **2019**, *4*, 352–357.

[12] J. H. Baek, T. M. Gill, H. Abroshan, S. Park, X. Shi, J. Nørskov, H. S. Jung, S. Siahrostami, X. Zheng, *ACS Energy Lett.* **2019**, *4*, 720–728.

[13] S. R. Kelly, X. Shi, S. Back, L. Vallez, S. Y. Park, S. Siahrostami, X. Zheng, J. K. Nørskov, *ACS Catal.* **2019**, *9*, 4593–4599.

[14] S. Mavrikis, M. Göltz, S. Rosiwal, L. Wang, C. Ponce de León, *ACS Appl. Energy Mater.* **2020**, *3*, 3169–3173.

[15] L. Li, Z. Hu, J. C. Yu, *Angew. Chemie - Int. Ed.* **2020**, *59*, 20538–20544.

[16] C. Zhang, R. Lu, C. Liu, L. Yuan, J. Wang, Y. Zhao, C. Yu, *Adv. Funct. Mater.* **2021**, *31*, 2100099.

[17] K. Dong, J. Liang, Y. Wang, Y. Ren, Z. Xu, H. Zhou, L. Li, Q. Liu, Y. Luo, T. Li, A. M. Asiri, Q. Li, D. Ma, X. Sun, *Chem Catal.* **2021**, DOI: 10.1016/j.checat.2021.10.011.

[18] C. Xia, S. Back, S. Ringe, K. Jiang, F. Chen, X. Sun, S. Siahrostami, K. Chan, H. Wang, *Nat. Catal.* **2020**, *3*, 125–134.

[19] S. Mavrikis, M. Göltz, S. C. Perry, F. Bogdan, P. K. Leung, S. Rosiwal, L. Wang, C. P. de León, *ACS Energy Lett.* **2021**, *6*, 2369–2377.

[20] D. Shi, L. Liu, Z. Zhai, B. Chen, Z. Lu, C. Zhang, Z. Yuan, M. Zhou, B. Yang, N. Huang, X. Jiang, *J. Mater. Sci. Technol.* **2021**, *86*, 1–10.

[21] P. Zhu, Y. Zhao, *Mater. Chem. Phys.* **2019**, *233*, 60–67.

[22] X. Shi, S. Back, T. M. Gill, S. Siahrostami, X. Zheng, *Chem* **2021**, *7*, 38–63.

[23] A. Zielinski, M. Cieslik, M. Sobaszek, R. Bogdanowicz, K. Darowicki, J. Ryl, *Ultramicroscopy* **2019**, *199*, 34–45.

[24] L. A. Hutton, J. G. Iacobini, E. Bitziou, R. B. Channon, M. E. Newton, J. V. Macpherson, *Anal.*

Chem. **2013**, *85*, 7230–7240.

[25] R. Bogdanowicz, M. Ficek, N. Malinowska, S. Gupta, R. Meek, P. Niedziałkowski, M. Rycewicz, M. Sawczak, J. Ryl, T. Ossowski, *J. Electroanal. Chem.* **2020**, *862*, 114016.

[26] T. M. Gill, L. Vallez, X. Zheng, *ACS Energy Lett.* **2021**, *6*, 2854–2862.

[27] D. M. Shub, M. F. Reznik, V. V. Shalaginov, *Sov. Electrochem.* **1985**, *21*, 878–882.

[28] A. Kapałka, G. Fóti, C. Comninellis, *Electrochim. Acta* **2007**, *53*, 1954–1961.

[29] A. Kapałka, G. Fóti, C. Comninellis, *Electrochem. commun.* **2008**, *10*, 607–610.

[30] M. H. P. Santana, L. A. D. Faria, J. F. C. Boodts, *Electrochim. Acta* **2005**, *50*, 2017–2027.

[31] F. Beck, H. Krohn, W. Kaiser, M. Fryda, C. P. Klages, L. Schäfer, *Electrochim. Acta* **1998**, *44*, 525–532.

[32] D. Gandini, E. Mahé, P. A. Michaud, W. Haenni, A. Perret, C. Comninellis, *J. Appl. Electrochem.* **2000**, *30*, 1345–1350.

[33] P. A. Michaud, M. Panizza, L. Ouattara, T. Diaco, G. Foti, C. Comninellis, *J. Appl. Electrochem.* **2003**, *33*, 151–154.

[34] D. A. García-Osorio, R. Jaimes, J. Vazquez-Arenas, R. H. Lara, J. Alvarez-Ramirez, *J. Electrochem. Soc.* **2017**, *164*, E3321.

[35] D. A. García-Osorio, J. Vazquez-Arenas, R. Jaimes, *J. Electrochem. Soc.* **2018**, *165*, J3101.

[36] W. Zhang, X. Chen, Y. Wang, L. Wu, Y. Hu, *ACS Omega* **2020**, *5*, 22465–22474.

[37] J. Kochany, E. Lipczynska-Kochany, *Chemosphere* **1992**, *25*, 1769–1782.

[38] E. V. Bakhmutova-Albert, H. Yao, D. E. Denevan, D. E. Richardson, *Inorg. Chem.* **2010**, *49*, 11287–11296.

[39] E. Illés, A. Mizrahi, V. Marks, D. Meyerstein, *Free Radic. Biol. Med.* **2019**, *131*, 1–6.

[40] Y. Xue, Y. Wang, Z. Pan, K. Sayama, *Angew. Chemie Int. Ed.* **2021**, *60*, 10469–10480.

[41] C. Liang, B. He, *Chemosphere* **2018**, *198*, 297–302.

[42] C. S. Christensen, S. Brødsgaard, P. Mortensen, K. Egmose, S. A. Linde, *J. Environ. Monit.* **2000**, *2*, 339–343.

[43] T. M. Gill, X. Zheng, *Chem. Mater.* **2020**, *32*, 6285–6294.

[44] J. Liang, Y. Wang, Q. Liu, Y. Luo, T. Li, H. Zhao, S. Lu, F. Zhang, A. M. Asiri, F. Liu, D. Ma, X. Sun, *J. Mater. Chem. A* **2021**, *9*, 6117–6122.

[45] Z. Xu, J. Liang, Y. Wang, K. Dong, X. Shi, Q. Liu, Y. Luo, T. Li, Y. Jia, A. M. Asiri, Z. Feng, Y. Wang, D. Ma, X. Sun, *ACS Appl. Mater. Interfaces* **2021**, *13*, 33182–33187.

[46] K. Dong, J. Liang, Y. Wang, Z. Xu, Q. Liu, Y. Luo, T. Li, L. Li, X. Shi, A. M. Asiri, Q. Li, D. Ma, X. Sun, *Angew. Chemie - Int. Ed.* **2021**, *60*, 10583–10587.

[47] Z. Deng, C. Ma, S. Yan, K. Dong, Q. Liu, Y. Luo, Y. Liu, J. Du, X. Sun, B. Zheng, *J. Mater. Chem. A* **2021**, *9*, 20345–20349.

[48] L. Zhang, J. Liang, L. Yue, Z. Xu, K. Dong, Q. Liu, Y. Luo, T. Li, X. Cheng, G. Cui, B. Tang, A. A. Alshehri, K. A. Alzahrani, X. Guo, X. Sun, *Nano Res.* **2022**, *15*, 304–309.

Table of Contents

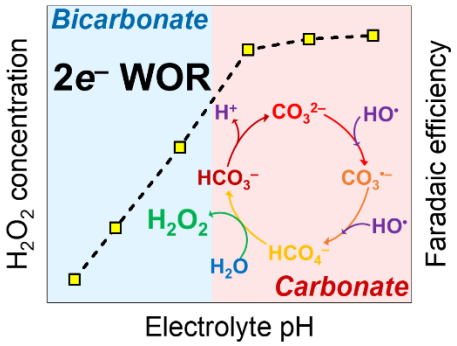

Optimising anodic H_2O_2 electrosynthesis: Carbonate-based electrolytes are found to considerably enhance hydrogen peroxide production via the two-electron water oxidation reaction, with notable Faraday efficiencies attained when using boron doped diamond anodes in highly concentrated potassium carbonate aqueous solutions.